Mid-Infrared Silicon Photonics for Communications

Goran Z. Mashanovich, Wei Cao, Zhibo Qu, Ke Li,
David J. Thomson, Milos Nedeljkovic
Optoelectronics Research Centre
University of Southampton
Southampton, Hampshire, SO17 1BJ, UK
g.mashanovich@soton.ac.uk

David Hagan, Andrew P. Knights
Department of Engineering Physics
McMaster University
Hamilton, Ontario L8 S 4L7, Canada

Abstract— **The mid-infrared wavelength region is important for a number of application areas, two of which are optical fibre and free space communications. Silicon photonics can provide inexpensive photonic chips for such applications due to excellent electronic and photonic properties. In this paper, the realisation of active silicon and germanium photonic devices for the mid-infrared spectral region are given. High speed Si depletion type modulators, Si and Ge injection modulators operating at wavelengths up to 8 micrometers, and high speed Si detectors are presented. These devices are integrated with drivers and amplifiers and show very good performance, e.g. data rate in excess of 20 Gb/s.**

Keywords-component; silicon, germanium, photonics, mid-infrared, modulator, detector.

I. INTRODUCTION

The mid-infrared (MIR) wavelength range (2-20 μm) has attracted lot of attention recently. This is mainly due to a number of molecules and substances having very strong absorption bands in this spectral range and hence photonic devices operating in the MIR can offer sensitive and selective sensors for healthcare, environmental monitoring, industrial process control, defense and security, to mention a few. On the other hand, the MIR has two atmospheric transmission windows (3-5 and 8-14 μm) and free space communications operating in these wavelength ranges can be developed.

Due to an exponential increase in data traffic new spectral regions will be needed. The 2 μm wavelength range is attractive due to the development of low loss optical fibres and thulium doped fibre amplifiers (TDFA) in this range. To address this future need, we have developed high speed Si modulators and detectors, as well as passive photonic devices. We have also theoretically investigated modulation in Si and Ge at longer wavelengths and experimentally verified them using Si and Ge injection modulators at longer wavelengths. All these devices have been fabricated using Silicon-on-Insulator (SOI) and Ge-on-Si (GOS) material platforms.

In Section II passive SOI and GOS devices are introduced, Section III presents different types of Si and Ge modulators, Section IV shows the realisation of a Si MIR detector, and finally conclusions are given in Section V.

II. PASSIVE SI AND GE DEVICES

The SOI platform is the most popular platform in the near-IR (NIR) wavelength range. However, due to high material loss of SiO_2 [1], this platform cannot be used beyond 4 μm [2]. We have shown in a number of publications that MIR SOI devices can match performance of much more mature SOI NIR counterparts if operating beyond 4 μm [e.g. 3-7]. Low loss waveguides (~1 dB/cm), couplers, splitters (0.1 dB/splitter), interferometers, and spectrometers have been demonstrated. These devices have been used for subsequent demonstrations of active devices and for integrated circuits for communications and sensing.

For wavelengths beyond 4 μm, we have developed a subwavelength suspended Si platform and experimentally demonstrated a library of passive devices operating at wavelengths up to 7.7 μm, reaching the transparency limit of Si [8-10]. The waveguide propagation loss was as low as 0.8 dB/cm, bend loss 0.005 dB/bend, and multimode interference (MMI) splitter and Mach Zehnder interferometer (MZI) insertion losses were smaller than 0.5 and 1 dB, respectively.

For even longer wavelengths (up to 13 μm) we have developed a low loss Ge-on-Si platform [e.g. 11] and demonstrated photonic devices such as MMIs, MZIs, grating couplers, Vernier ring resonator filters and sensors [e.g. 11-14]. We have also investigated nonlinear effects in Ge waveguides [15-16]. The waveguide loss was 0.6 dB/cm at 3.8 μm [11], 2.5 dB/cm at 7.5 μm, but it increased to ~15 dB/cm at 8.5 μm [17]. We are currently investigating the reasons for such a high loss at longer wavelengths but in the meantime we have developed a suspended Ge platform (Fig. 1).

First, Ge was grown on a thin SOI wafer by reduced pressure chemical vapour deposition (RPCVD). A rib Ge waveguide was then formed by lithography and etching, holes on both sides of the rib were etched, and finally hydrofluoric (HF) acid and tetramethylammonium hydroxide (TMAH) used to remove SiO_2 and thin Si layers, respectively. Loss of 2.65 dB/cm was measured at a wavelength of 7.7 μm [18]. Further work is underway to demonstrate such waveguides at wavelengths up to 13 μm, as well as to fabricate subwavelength variation of the suspended Ge.

This work was supported by EPSRC in the UK through the following grants: EP/N00762X/1, EP/L021129/1, EP/N013247/1 and EP/L01162X/1.

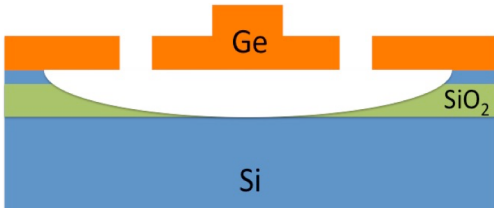

Figure 1. Suspended Ge rib waveguide.

In summary, there are several group IV based platforms that can be used in the MIR. In our work shown in sections III and IV we have used SOI and GOS as the most popular platforms to demonstrate optical modulators and detectors in the MIR.

III. SILICON MODULATORS

Due to its centro-symmetric crystalline structure, silicon does not have Pockels effect and therefore optical modulation is usually performed through thermal or carrier effects. Hybrid modulators have also been shown using III-V bonded devices on Si, polymers, graphene or via integration with $LiNbO_3$. Whilst these hybrid solutions can result in efficient modulators, they are not CMOS compatible and would find significant barriers for large volume markets. In this section, CMOS compatible MIR solutions are presented, namely thermal modulators in Si, and carrier effect (plasma dispersion) modulators in Si and Ge.

A. *Thermal modulators*

Silicon has a large thermo-optic effect (change in refractive index with temperature) of dn/dT = 1.70 × 10^{-4} °C^{-1} at a wavelength of 3.8 μm, which is in many cases undesirable characteristic of Si as resonant devices (e.g. ring resonators) change their responses significantly with temperature. On the other hand, this large thermo-optic coefficient can be used to modulate optical response although with low bandwidth. We have investigated modulators that were based on heaters placed above one arm of a MZI (Fig. 2). The MZI used SOI rib waveguides with silicon height H=400 nm, waveguide width W=1300 nm, etch depth D=220 nm, and buried oxide layer (BOX) thickness H_{BOX}=2 μm. 1×2 MMIs with tapered input and output ports are used as the splitter/coupler for the MZI.

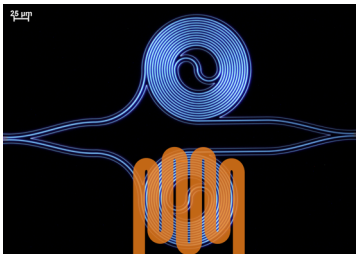

Figure 2. MZI with Si spiral waveguides in both arms (blue) and a heater in one arm (orange).

An aluminium heater, which acts as a phase shifter, is placed above one of the MZI arms, and because there is high optical absorption in metals a SiO_2 layer is used to isolate the heater from the optical mode. MZIs exhibited modulation depths of up to 30.5 dB, insertion losses of 1.3-2.2 dB, -3dB bandwidths of up to 23.8kHz, and power consumption of 47 mW [19]. For high speed application plasma dispersion effects need to be used.

B. *Plasma dispersion effects in Si*

The free-carrier plasma effect (abbreviated here as FCE for free-carrier effect) relies on altering the electron and hole concentration in crystalline silicon or germanium, which alters the absorption coefficient ($\Delta\alpha$) and the refractive index (Δn) of the bulk material. The electroabsorption and electrorefraction due to a change in charge carrier concentrations can be calculated from simple expressions, that we have derived for Si and Ge [20,21] for $\Delta\alpha$ vs ΔN_e and ΔN_h, and Δn vs ΔN_e and ΔN_h at near-infared (NIR) and mid-infrared (MIR) wavelengths. These expressions have been calculated from absorption spectra of doped silicon and germanium wafers, and from using Kramers-Kronig (KK) equations to calculate the refractive index change at different charge carrier concentrations. The main conclusion from the theoretical work we have conducted is that FCE is generally larger in Ge than in Si. Also at longer wavelengths modulators exploiting free-carrier electro-absorption are likely to be more effective than those using electrorefraction. There are three main methods to utilise FCE: carrier injection, carrier accumulation, and carrier depletion. Modulators based on the first are the simplest to fabricate, and those based on the the third have the highest bandwidth. We have therefore used them at longer wavelengths and for high bandwidth modulators at the 2 μm wavelength range, respectively.

C. *Si depletion modulators*

Using the equations reported in [20] we have designed a depletion phase shifter, shown in Fig. 3, and implemented it in both MZI and ring resonator configurations. 220 nm SOI was used and wide band Y-splitters in MZMs such that realized modulators could operate at both 1550 nm and 1950 nm. Ring resonators were integrated with drivers designed by our group.

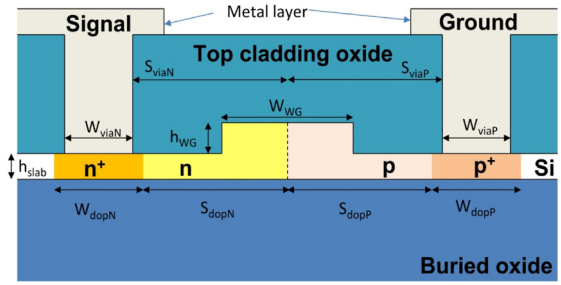

Figure 3. Si depletion modulator

During the design process, two important dimension parameters have been swept to analyse their effects. The first is the separation between the high doping sections and the optical waveguide core. When varying the doping separation, there is a trade-off between device bandwidth and free carrier loss. The

device bandwidth rises as the high doping separation decreases, due to reduced access resistance. However, when the high doping is too close to the waveguide core, the overlap between the optical mode and free carriers in the high doping region increases, resulting in significant optical loss. Therefore, a trade-off between device bandwidth and device loss should be considered.

The PN junction position is the second major parameter. the device has the lowest loss and highest efficiency when it is placed near the centre of the waveguide, because the maximum overlap of the optical mode and depletion region is achieved. The bandwidth, however, increases when the junction position is close to the edge of the waveguide core, because in this case the PN junction is partially in the slab region of the waveguide and has a reduced cross-section compared to in the core region. This results in lower capacitance and hence higher bandwidth. However, achieving this condition comes at the cost of significantly higher loss and lower efficiency. If the doping separation is chosen properly, the simulated bandwidth should be greater than 75 GHz regardless of junction position. In our design, we chose a 0 nm junction offset.

Fabricated device modulation efficiency at 4 V reverse bias was 2.68 V·cm for 1950 nm and 2.02 V·cm for 1550 nm. The slightly lower efficiency at 1950 nm was due to a larger optical mode caused by a lower overlapping factor with the depletion region in the PN junction. The device operated at a data rate of 20 Gbit/s with an extinction ratio of 5.8 dB and 30 Gbit/s with an extinction ratio of 7.1 dB for 1950 nm and 1550 nm, respectively [22]. The wavelength should have very little effect on the bandwidth, and the difference was mainly caused by the bandwidth limit of our 2 µm measurement setup, due mostly to the bandwidth limit of the high-speed detector used. The ring modulator operated in carrier depletion mode with 43 pm resonance shift under 4 V reverse bias. Driven by a low power integrated driver the ring operated in a hybrid carrier injection and depletion mode at a data rate of 3 Gbit/s with extinction ratio of 2.30 dB and power consumption of 2.38 pJ/bit in the 2 µm wavelength range.

D. Si injection modulators

To demonstrate injection Si modulators at longer wavelength and to compare our theoretical predictions with experimental results we used 340 nm SOI wafers with the buried oxide layer thickness of 2 µm, to fabricate rib waveguides 1175 nm wide and etched 240 nm (Fig. 4). Simulations using the Lumerical Mode Solutions EME solver showed that these waveguides would support the fundamental TE mode only. The SiO_2 top cladding thickness was 1 µm. The P++ and N++ Ohmic contact regions had doping concentrations of 1e20 cm^{-3} of boron and 9e19 cm^{-3} of phosphorus, respectively. The Si had a p-type background doping of 1.5e17 cm^{-3}. Both electroabsorption (spiral waveguide) and electrorefraction (MZI) modulators were fabricated and characterised.

The electroabsorption modulator (EAM) achieved a DC modulation depth of 34 dB and an AC data rate of 60 Mbit/s, while the electrorefraction modulator achieved a DC modulation depth of 22.2 dB with a $V_\pi L_\pi$ of 0.052 V.mm, and an AC data rate of 125 Mbit/s [23]. The MZI modulator measurements indicated that the free carrier effect equations for this wavelength accurately predicted the correlation between absorption coefficient and refractive index changes due to a change in free carrier concentration, while the measurements of excess loss from doping indicated that the equations also reasonably accurately predicted the absolute value of the free carrier absorption.

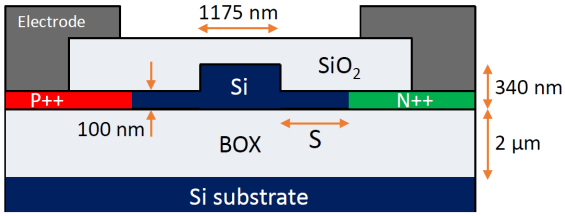

Figure 4. SOI *pin* structure

E. Ge injection modulators

We have also investigated mid-infrared electro-optic modulators based on the Ge-on-Si platform at wavelengths up to 8 µm. The cross section of the Ge phase shifter is shown in Fig. 5. A fabricated 1-mm-long EAM exhibited a DC modulation depth in excess of 35 dB at 3.8 µm wavelength, and a MZM with a 1–mm-long phase shifter at the same wavelength had a modulation depth of 13 dB with a $V_\pi \cdot L$ of 0.47 V·cm. When driven by a RF signal, 60 MHz OOK modulation was demonstrated in both the EAM and MZM devices. An EAM device has also been demonstrated at a wavelength of 8 µm, with a 2.5 dB modulation depth for a 7 V DC forward bias in a 2–mm-long PIN diode [24]. The measurements indicated that the injected free carrier absorption was more than 4.9 times greater at 8 µm than at 3.8 µm for the same carrier concentration, which was consistent with the theoretical predictions of [21]. The modulation efficiency of all of these modulators would be expected to increase significantly with optimisation of the Ohmic contact separation and with improved Ohmic contact fabrication.

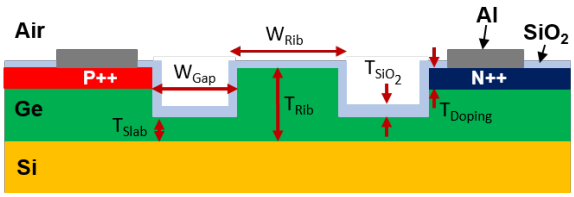

Figure 5. GOS *pin* structure.

IV. DETECTORS

One of the most important devices for integrated photonic circuits is a photodetector. A CMOS compatible waveguide integrated detector at the 2 µm range would complement III-V and fibre optic sources, TDFA and modulators reported in the previous section.

We have utilised mid-bandgap absorption due to presence of divacancies in the silicon crystalline structure, as a result of inert ion implantation of boron into silicon. The most distinctive feature of the device fabrication process was the simplicity, since no heterogeneous integration was necessary. The detectors consisted of 220nm thick SOI waveguides with a lateral *pin* junction, similar to the injection Si modulators from section III. An etched window in the oxide cladding above the waveguide served as a mask to target the intrinsic region of the *pin* diode with the inert implantation. The heavily doped *p* and *n*-regions of the device were positioned 300 nm from the waveguide sidewall to manage propagation loss. Aluminum contacts were positioned several microns away from the waveguide. Coupling light from an external fibre to the detector was accomplished by inverted-taper waveguides that extend to the edge of the chip and provided broadband access. The width of the couplers tapered linearly from 1 μm to 180 nm over a length of 200 nm and terminated within a few microns of the sample edge.

A 1 mm long detector showed a 3 dB bandwidth of 12.5 GHz while the 200 μm long device showed 15 GHz. The measured capacitance of our 1 mm long detector was 260 ± 10 fF. With a 50 Ω load this provided an *RC* limited bandwidth of ~ 12 GHz. The detector operated in avalanche mode at a date rate of up to 28 Gbit/s. External responsivity of the detector at 2 μm was 0.3 ± 0.02 A/W [25], and we expect further improvement with an optimised waveguide and detector design to improve the modal confinement factor and reduce propagation loss.

V. Conclusions

We have shown several active devices realised in Si and Ge that operated in the MIR and that can find application if future MIR communications. Although the field of silicon MIR photonics is still in its infancy, the reported results show much promise for the realisation of efficient components and integrated circuits for several important application areas.

References

[1] R. Soref "Mid-infrared photonics in silicon and germanium," Nat. Photon., vol. 4, pp. 495–497, 2010.

[2] M. M. Milosevic *et al.*, "Silicon waveguides and devices for the mid-infrared," Appl. Phys. Lett., vol. 101, 121105, 2012.

[3] M. Nedeljkovic *et al.*, "Silicon photonic devices and platforms for the mid-infrared" Opt. Mat. Express, vol. 3, pp. 1205–1214, 2013.

[4] G. Z. Mashanovich *et al.*, "Silicon photonic waveguides and devices for near- and mid-IR applications," J. Sel. Topics Quantum Electron., vol. 21, 8200112, 2015.

[5] M-S. Rouifed *et al.*, "Ultra-compact MMI-based beam splitter demultiplexer for the NIR/MIR wavelengths of 1.55 μm and 2 μm," Opt. Express, vol. 25, pp. 10893-10900, 2017.

[6] M. Nedeljkovic, A. V. Velasco, A. Z. Khokhar, A. Delâge, P. Cheben, and G. Z. Mashanovich, "Mid-infrared silicon-on-insulator Fourier-transform spectrometer chip," IEEE Photon. Technol. Lett., vol. 28, pp. 528-531, 2016.

[7] M. Muneeb *et al.*, "Demonstration of silicon-on-insulator mid-infrared spectrometers operating at 3.8μm," Opt. Express, vol. 21, pp. 11659–11669, 2013.

[8] J. Soler Penades *et al.*, "Suspended SOI waveguide with sub-wavelength grating cladding for mid-infrared," Opt. Lett., vol. 39, pp. 5661-5664, 2014.

[9] J. Soler Penades *et al.*, "Suspended silicon mid-infrared waveguide devices with subwavelength grating metamaterial cladding," Opt. Express, vol. 24, pp. 22908-22916, 2016.

[10] J. Soler Penades *et al.*, "Suspended silicon waveguides for long-wave infrared wavelengths," Opt. Lett., vol. 43, pp. 795-798, 2018.

[11] M. Nedeljkovic *et al.*, "Surface grating coupled low loss Ge-on-Si rib waveguides and multimode interferometers," IEEE Photon. Technol. Lett., vol. 27, pp. 1040-1043, 2015.

[12] C. Alonso-Ramos *et al.*, "Germanium-on-silicon mid-infrared grating couplers with low-reflectivity inverse taper excitation," Opt. Lett., vol. 41, pp. 4324-4327, 2016.

[13] B. Troia *et al.*, "Germanium-on-silicon Vernier-effect photonic microcavities for the mid-infrared," Opt. Lett., vol. 41, pp. 610-613, 2016.

[14] V. Mittal et al., "Waveguide mid-infrared absorption spectroscopy of proteins in the spectral fingerprint region," unpublished

[15] L. Shen *et al.*, "Mid-infrared all-optical modulation in low loss germanium-on-silicon waveguides," Opt. Lett., vol. 40, pp. 268–271, 2015.

[16] L. Shen *et al.*, "Two-photon absorption and all-optical modulation in germanium-on-silicon waveguides for the mid-infrared," Opt. Lett., vol. 40, pp. 2213-2216, 2015.

[17] M. Nedeljkovic *et al.*, "Germanium-on-silicon waveguides operating at mid-infrared wavelengths up to 8.5 μm," Opt. Express, vol. 25, pp. 27431-27441, 2017.

[18] A. Osman *et al.*, "Suspended low-loss germanium waveguides for the longwave-infrared," Opt. Lett., vol. 43, pp. 5997-6000, 2018.

[19] M. Nedeljkovic *et al.*, "Mid-infrared thermo-optic modulators in SOI," IEEE Photon. Technol. Lett., vol. 26, pp. 1352-1355, 2014.

[20] M. Nedeljkovic, R. Soref, and G. Z. Mashanovich, "Free-carrier electro-refraction and electro-absorption modulation predictions for silicon over the 1-14μm wavelength range," IEEE Photon. J., vol. 3, pp. 1171-1180, 2011.

[21] M. Nedeljkovic, R. Soref, and G. Z. Mashanovich, "Predictions of free-carrier electroabsorption and electrorefraction in germanium," IEEE Photon. J., vol. 7, 2419217, 2015.

[22] W. Cao *et al.*, "High speed modulators in silicon-on-insulator for the 2 μm wavelength band," Optica, vol. 5, pp. 1055-1062, 2018.

[23] M. Nedeljkovic *et al.*, "Silicon-on-insulator free-carrier injection modulators for the mid-infrared," Opt. Lett., in press.

[24] T. Li *et al.*, "Ge-on-Si modulators operating at mid-infrared wavelengths up to 8 μm," unpublished.

[25] J. J. Ackert *et al.*, "High-speed detection above the telecommunication windows with monolithic silicon photodiodes," Nat. Photon., vol. 9, pp. 393-396, 2015.